

1           A hydrogel beads based platform for single-cell  
2 phenotypic analysis and digital molecular detection

3           Yanzhe Zhu, Jing Li, Xingyu Lin, Xiao Huang, and Michael R. Hoffmann\*

4                           Linde+Robinson Laboratories

5                           California Institute of Technology

6                           Pasadena California 91125 USA

7           \* Correspondence and requests for materials should be addressed to MRH

8                           Tel: 626-395-4391 EM: [mrh@caltech.edu](mailto:mrh@caltech.edu)

9

10

11

12

13

14

15

16

17

To be Submitted to: *Biorxiv*

18

November, 2019

## Abstract

19           Microfluidic platforms integrating phenotyping and genotyping approaches have the  
20 potential to advance the understanding of single cell genotype-to-phenotype correlations. These  
21 correlations can play a key role in tackling antibiotic heteroresistance, cancer cell heterogeneity,  
22 and other related fundamental problems. Herein, we report a novel platform that enables both high-  
23 throughput digital molecular detection and single-cell phenotypic analysis, utilizing nanoliter-  
24 sized biocompatible polyethylene glycol hydrogel beads produced by a convenient and disposable  
25 centrifugal droplet generation device. The hydrogel beads have been demonstrated enhanced  
26 thermal stability, and achieved uncompromised efficiencies in digital polymerase chain reaction,  
27 digital loop-mediated isothermal amplification, and single cell phenotyping. The crosslinked  
28 hydrogel network highlights the prospective linkage of various subsequent molecular analyses to  
29 address the genotypic differences between cellular subpopulations exhibiting distinct phenotypes.  
30 Our platform shows great potential for applications in clinical practice and medical research, and  
31 promises new perspectives in mechanism elucidation of environment-evolution interaction and  
32 other basic research areas.

## Introduction

33           Microfluidic single cell techniques have enabled observations of rare genotypes or  
34 phenotypes within a cell population and thus ubiquitous cell heterogeneity (1-3). The phenotypic  
35 diversity exhibited by supposedly genetically identical cells boosts the population adaptability  
36 under selection pressures, and thus raises concerns in fields spanning from clinical practice to  
37 medical research on infectious diseases and cancers (4, 5), etc. For example, less susceptible  
38 pathogenic bacterial subpopulations originally consist  $10^{-2}$  to  $10^{-6}$  of the overall population that  
39 can be amplified during antibiotic exposure. The subsequent increase in the resistant subpopulation  
40 may eventually lead to the failure of an antibiotic treatment (6). Hypotheses for the underlying  
41 molecular mechanisms involving the stochasticity of genetic mutation, gene expression, and  
42 protein regulation (7-9), however, remain hard to test in dynamically changing cell subpopulations,  
43 partly due to the absence of appropriate single cell experimental technique (10). The need to better  
44 understand cell heterogeneity motivates the development of new techniques that link the single-  
45 cell phenotype with its *in situ* molecular information.

46           As an emerging class of technologies, water-in-oil droplet-based microfluidic platforms  
47 have been well developed for high-throughput phenotypic and molecular analyses at single cell or  
48 single molecule resolution (3, 11). Nonetheless, due to the rare and transient nature of cell  
49 heterogeneity events, population-averaged molecular analyses would most likely fail to directly  
50 explain the characterized phenotypes, even if all analyses are conducted at single cell or molecular  
51 resolution (6, 12). Meanwhile, incorporating a crosslinked hydrogel network into the aqueous  
52 phase theoretically provides a droplet-based platform with additional robustness by allowing  
53 reagent exchange (13). This strategy, therefore, has been explored for a range of hydrogel materials  
54 and crosslinking chemistry, including cooling-induced formation of agarose beads for digital

55 droplet polymerase chain reaction polymerase chain reaction (ddPCR) (14), ionic crosslinking of  
56 alginate beads for cell encapsulation and DNA extraction (15, 16), UV-initiated polyethylene  
57 glycol (PEG) beads for cell encapsulation (17). Such platforms have demonstrated to be effective  
58 in either phenotyping or molecular analysis, while the material and/or initiation method would be  
59 intrinsically incompatible with the combination of both. For example, temperature manipulation  
60 or UV radiation might affect the phenotype and genotype of encapsulated cells (18), and alginate  
61 is a well-known PCR inhibitor (19). PEG crosslinked by a thiol-Michael addition reaction between  
62 the bioinert acrylate and thiol groups has been attempted in bulk analyses and is among the most  
63 promising solutions (20, 21), but it is yet to be developed for our specific purpose. The main  
64 obstacle may lie in the fast and spontaneous gelation, which would be detrimental to traditional  
65 expensive microfluidic droplet generation approaches.

66       Herein, we report a novel PEG hydrogel bead-based platform, which is validated for both  
67 single-cell phenotypic analysis and molecular detection (**Figure 1a-b**). To solve the challenge  
68 posted by the fast thiol-Michael addition gelation chemistry, we developed a disposable centrifugal  
69 device for droplet generation (**Figure 1c**). We demonstrated the effectiveness of nucleic acid  
70 amplification detections, including PCR and loop-mediated isothermal amplification (LAMP),  
71 through further crosslinking generated droplets into PEG hydrogel as PEG hydrogel beads  
72 (Gelbeads). Compared to ddPCR and ddLAMP, Gelbead-based digital PCR and LAMP (gdPCR  
73 and gdLAMP) were found to exhibit enhanced thermal stabilities and uncompromised  
74 amplification efficiencies. Gelbeads were also demonstrated effective for single cell encapsulation  
75 and phenotyping within 4 hr for tested bacteria. We envision that this platform will be of broad  
76 interest to researchers from many fundamental fields. The Gelbead platform reported here for the  
77 first time promises unprecedented capabilities for investigation of cell heterogeneity.

## Results

### 78 **Development of the disposable droplet generation device**

79 Microfluidic-based droplet generation methods generally require special fabrication  
80 facilities to fabricate sub-100  $\mu\text{m}$  channels and involve complicated operation, such as syringe  
81 pump-driven T-junctions fabricated by photolithography and centrifugally driven labs-on-a-disc  
82 fabricated by micro milling and hot embossing (22, 23). These traditional methods are not  
83 compatible with Gelbead generation due to fast clogging imposed by the thiol-Michael addition  
84 chemistry. The bulk PEG crosslinking experiments showed that the time frame for droplet  
85 generation before gelation was as short as 8.5 min with the chosen hydrogel concentration at 7.5  
86 w/v% (**Supplementary Note 1, Table S1**). In order to easily generate Gelbeads within minutes  
87 without clogging expensive microfluidic equipment, we designed a disposable device using  
88 affordable commercial components (**Figure 2a**). The device utilized a dispensing blunt needle  
89 with a bent tip. The bent-tipped needle was then set into a 1.5-mL microcentrifuge tube with oil to  
90 establish the physics for centrifugal droplet generation. With centrifugal acceleration, the aqueous  
91 phase is forced into the fluorinated oil phase by the elevated pressure difference between the  
92 reservoir surface and the narrow inlet. The fluorinated oil phase with a higher density pinches off  
93 the aqueous droplets, which then float to the air-oil interface.

94 Standard 20  $\mu\text{L}$  LAMP mix with unquenched calcein was dispersed in fluorinated oil  
95 (online methods) and characterized using a fluorescence microscope to study the droplet  
96 generation performance of the device (**Figure 2b**). The average droplet size was tunable from 99  
97  $\mu\text{m}$  to 334  $\mu\text{m}$  and the coefficient of variance (CV) was minimized to 5%, by varying the oil phase  
98 volume, centrifugal acceleration, and the needle gauge as shown in **Figure 2c-f**. Smaller droplets  
99 with slightly larger size distribution (**Figure 2e**) were produced by increasing the centrifugal

100 acceleration, which provided a greater pressure difference to drive the aqueous phase inflow. The  
101 larger CV in **Figure 2e** was likely due to the unstable flow during initial acceleration, which can  
102 be alleviated by adding more oil (**Figure 2c**) to reduce the oil phase height variation and limit the  
103 amount of aqueous phase inlet during acceleration. Among all tested conditions, the optimal was  
104 found to be a combination of 34 Ga needles, 80  $\mu\text{L}$  oil phase, and 150 g centrifugation run for 5  
105 min and droplets were produced at an average diameter of 175  $\mu\text{m}$  in 5 min with minor trial-to-  
106 trial difference, which was found to be comparable to other microfluidic methods such as  
107 centrifugal lab-on-a-disk (22) and polymer-tube micronozzles (24) (**Supplementary Note 2**). For  
108 droplets of a diameter of 175  $\mu\text{m}$ , each standard 20  $\mu\text{L}$  reaction could theoretically produce  $\sim 10^4$   
109 droplets. Based on this calculated compartmentalization, the dynamic range is theoretically from  
110 0.5 to  $3 \times 10^3$  target copies or cells per  $\mu\text{L}$ , and the detection limit is 0.1 copies or cells per  $\mu\text{L}$  (25).

### 111 **Gelbead generation and thermal stability characterization**

112 The Gelbead and droplet generation performance were assessed using various reaction  
113 matrices including culture media, PCR mix, and LAMP mix, under the optimized condition  
114 reported in the previous section (**Figure 3a**). The average diameter of generated Gelbeads was  
115 found to range from 145  $\mu\text{m}$  to 217  $\mu\text{m}$  with a CV from 3.6 % to 7.6 %. The observed variations  
116 were likely due to viscosity differences and interfacial property changes in different reaction  
117 matrices. It should be noted that the culture media alone was not able to sustain as droplets or  
118 Gelbeads in the fluorinated oil by 5% FluoroSurfactant. Bovine serum albumin (BSA), a protein  
119 commonly used as an additive to protect essential molecules (fatty acids, amino acids, etc.) in  
120 culture media (26), was added to the aqueous phase as an additional surfactant to modify interfacial  
121 properties and thus prevent the droplet merging. For the PCR reaction matrix, the generated  
122 Gelbeads had a larger CV than droplets. We assume that the presence of PEG hydrogel may have

123    disturbed the surfactant-stabilized aqueous-oil interface, by inducing interfacial adsorption of  
124    additional charged species such as thiolate, magnesium ions, etc. In summary, the observed sizes  
125    and CVs of droplets and Gelbeads were considered acceptable for our assays. In general, this  
126    generation device fulfills the requirements for Gelbead generation. The simple generation device  
127    may be used for applications for which a simple yet powerful compartmentalization method is  
128    needed.

129            The effect of PEG crosslinking on stabilizing the aqueous-in-oil compartments was  
130    evaluated. Thermodynamic instability of water-in oil droplets may impair the reliability of  
131    amplification processes such as PCR and LAMP that require extensive heating (22). Heating  
132    accelerates droplet merging and evaporation, which would affect the fluorescence reading by  
133    modifying concentrations of targets and reagents (e.g., salts and fluorescent dyes). The size  
134    distributions were investigated for droplets and Gelbeads before and after common heating  
135    protocols respectively for PCR and LAMP (online methods, **Figure 3b**). Compared to those before  
136    heating, droplets that had undergone PCR and LAMP heating increased in their CVs by 6.2% and  
137    3.5%, respectively. In addition, the heating resulted in a noticeably larger population with outlier  
138    sizes implying that extensive merging and evaporation had occurred. Following the same heating  
139    protocol as for the droplets, the Gelbeads exhibited much less of a change in size distribution (CV  
140    increased by 1.9% for PCR and 1.6% for LAMP), however the average Gelbead diameter  
141    decreased slightly. These results indicate that the stabilization effect achieved by crosslinked PEG  
142    was mainly by prevention of the merging of beads. Gelbeads used for the LAMP procedure had a  
143    more significant improvement in thermal stability due to PEG crosslinking than for the PCR  
144    procedure. We assume that, in the case of the PCR recipe, the combination of SuperMix and the  
145    oil phase from BioRad were chemically well-optimized for interfacial stability, leaving limited

146 room for improvement. This result therefore indicates that, other than modifying the surfactant  
147 composition or increasing surfactant concentration, hydrogel crosslinking could be an alternative  
148 strategy for maintaining the emulsion. Our results demonstrate that Gelbeads are a reliable  
149 platform for standalone heated digital analysis in terms of enhanced individual compartment  
150 integrity.

### 151 **Gelbead digital PCR (gdPCR)**

152 To validate the reliability of gdPCR, we compared gdPCR to digital PCR performed in  
153 droplets generated from a commercial recipe (represented as ddPCR, hereinafter) for amplification  
154 efficiency with DNA extracted from cultured *Salmonella* Typhi (*S. Typhi*). Previous use of  
155 hydrogels and PCR utilized polyacrylamide in the form of either a bulk phase hydrogel membrane  
156 as a quasi-digital PCR platform (27) or using hydrogel beads as a substrate for surface coating of  
157 primers (28, 29), which is an approach opposite to our concept. To the best of our knowledge,  
158 performing PCR inside crosslinked hydrogel beads has not been reported to date. Even in bulk  
159 membrane form, only 80% amplification efficiency was observed, which may be partially  
160 attributed to template damage by free radicals as suggested (27). In this study, a similar drop in  
161 amplification efficiency was observed in the Gelbeads compared to that in droplets (**Figure 4a**),  
162 even though the Michael addition chemistry between acrylate and thiol used in this study does not  
163 involve free radical formation. In this case, crosslinked hydrogel network may be responsible for  
164 the observed inhibition by limiting the diffusion of functional components such as ions, nucleic  
165 acids, and proteins, where the extent of the limitation relates to the size and charge of the  
166 component (30, 31). From effective diffusivity modeling (**Figure S1**), we reasoned that the most  
167 affected functional component might be DNA polymerase, which is the relatively large protein  
168 (~6 nm) responsible for building amplicons. For a fixed template concentration of 200 copies/ $\mu$ L



169 estimated by ddPCR, gdPCR assay performance was assessed with additional OneTaq polymerase  
170 supplied at varying concentrations of 0.025, 0.05, 0.1, 0.2 Units per reaction, as shown in **Figure**  
171 **4a**. Results showed that additional 0.025 Unit per reaction, 5% of the recommended OneTaq  
172 polymerase concentration per reaction, boosted the amplification efficiency the most. OneTaq  
173 polymerase concentrations supplied more or less than that showed inhibition to amplification  
174 efficiency, and gdPCR assay with additional 0.2 Unit per reaction was shown to be completely  
175 inhibited. We speculate that the observed trend was mainly due to the commercial SuperMix buffer  
176 conditions not optimized for the supplied OneTaq polymerase. While some additional polymerase  
177 compensated the reduced diffusivity of the SuperMix polymerase in hydrogel, the excess  
178 additional OneTaq polymerase might scavenge the essential ions for the original polymerase from  
179 SuperMix leading to amplification failure. With the optimized additional polymerase, gdPCR  
180 assays for serially diluted DNA with concentrations ranging from 2.5 to 600 copies/ $\mu$ L were then  
181 performed; typical images are shown in **Figure 4c-h (Supplementary Note 3)**. The image analysis  
182 results demonstrated that the amplification efficiency of gdPCR was comparable ( $k = 0.98 \pm 0.02$ ,  
183  $R^2 = 0.9979$ ) to that of ddPCR with the recipe adjustment (**Figure 4b**). The quantification results  
184 also correlated well with input DNA concentration (**Figure S2a**). It should be noted that the  
185 crosslinking inhibition effect eliminated in this case was for a 131 bp target gene (32), a typical  
186 size for detection of specific bacteria. Further optimization in polymerase or Supermix  
187 concentration would be required for other applications if a larger DNA fragment is targeted.

#### 188 **Gelbeads digital LAMP (gdLAMP)**

189 Gelbeads applied in digital LAMP were also investigated. LAMP has been an attractive  
190 emerging platform for molecular detection since it eliminates the need for thermocycling by  
191 utilizing a combination of 4 or 6 primers to achieve fast and specific detection (33). The heating

192 protocol of LAMP was fairly mild, however, severe Gelbead aggregation occurred for samples  
193 with target DNA but not for no-template controls (**Figure S3**) in preliminary experiments. This  
194 was supposedly due to the fact that LAMP produces a much larger amount of amplification  
195 products than PCR (33). The negatively charged amplified DNA may have affected interfacial  
196 tension when adsorbed to the interface. Aggregated Gelbeads showed apparent crosstalk, which  
197 rendered the assay invalid since the compartment independence assumption required for Poisson  
198 statistics was contradicted. The problem was relieved by adding 1.5 mg/mL BSA, a common real-  
199 time PCR additive, to prevent surface adsorption. However, it was still observed that positive  
200 Gelbeads tended to stick next to each other (**Figure 5a**). The observed radiative patterns in  
201 Gelbeads manifested the differential diffusivity of amplification products of varying size in  
202 crosslinked hydrogel network. A similar radiative pattern was observed by Huang et al. in LAMP  
203 performed in a hydrogel membrane (21). In our case, neither of the two radiative centers were at  
204 the connected interface, indicating that the stickiness may not have led to false positive Gelbeads  
205 within the time frame tested. The connection of positive Gelbeads was most likely the result of a  
206 change in interfacial tension caused by large amount of the negatively charged DNA produced  
207 during amplification. Further crosslinking breaking through the oil barrier would only occur when  
208 the positive Gelbeads encounter each other. In summary, the connected interface should not affect  
209 the quantification results. The gdLAMP quantifications for no-template control and serial diluted  
210 *S. Typhi* DNA ranging from 300 to  $1.2 \times 10^4$  copies/ $\mu$ L were then verified. Example images are  
211 shown in **Figure 5c-h**. The image analysis results demonstrated that the amplification efficiency  
212 of gdLAMP was similar ( $k = 1.01 \pm 0.01$ ,  $R^2 = 0.9996$ ) to that of ddLAMP (**Figure 5b**). However,  
213 both ddLAMP and gdLAMP gave concentration estimations ~2 orders of magnitude lower than  
214 input DNA concentration (**Figure S2b**). Further increases in the amplification efficiency would

215 likely require an improved primer design, which is out of the scope of this study. In summary, the  
216 results confirmed our hypothesis that the stickiness of positive Gelbeads do not considerably affect  
217 gdLAMP quantification, and demonstrated that the hydrogel network had a negligible inhibition  
218 effect on the digital LAMP assays that were performed.

### 219 **Gelbeads for cell phenotyping**

220 For single cell phenotyping, we first validated single cell encapsulation efficiency using  
221 *Salmonella* Typhimurium with green fluorescent protein (GFP). The cells were diluted to an  
222 average of 1 cell per Gelbead for counting the number of cells in each Gelbead (**Figure 6b**). At  
223 this cell concentration, theoretically, 34% of the compartments were occupied by single cells,  
224 which was the maximum following a Poisson distribution, 29% of the compartments encapsulated  
225 more than 1 cell, and 37% of the compartments contained no cells. As shown in **Figure 6a**, the  
226 observed number of encapsulated cells was close to the theoretical distribution. Gelbeads with high  
227 cell numbers were slightly less than predicted, possibly because some cells were located out of  
228 focus when imaged in spherical compartments at a high microscope objective. Since high  
229 throughput detection of stained cells within spherical compartments droplets or Gelbeads was  
230 challenging for fluorescence microscope imaging, we chose to employ cell metabolism indicator  
231 dye in Gelbead phenotyping experiments. As a resazurin-based dye used in bulk phenotyping  
232 assays of a wide range of cell lines, alamarBlue can be reduced by actively metabolizing cells into  
233 resorufin, whose bright red fluorescence can stain the whole compartment for visualization (34).  
234 Phenotyping of *S. Typhi* in Gelbeads was investigated by co-incubation of alamarBlue and *S.*  
235 *Typhi* in the culture media. The fluorescence of Gelbeads was monitored during the incubation for  
236 up to 4 hrs (**Figure 6d-h**). It was observed that Gelbeads appeared to be much brighter than the  
237 droplets were before incubation (**Figure S4**); this was possibly due to additional reduction of

238 resazurin by thiol group (35). We suppose that the interference by thiol groups would not affect  
239 the phenotyping results since the monomers were rigorously mixed and evenly distributed into  
240 Gelbeads. Gelbeads containing live cells would exhibit even brighter fluorescence in the presence  
241 of sufficient AlamarBlue. The quantitative performance of Gelbead phenotyping was verified by  
242 analysis of observed fractions of bright fluorescent Gelbeads (see online methods and **Figure S5**  
243 for thresholding) compared to the theoretical value, as shown in **Figure 6c**. 63% of Gelbeads were  
244 supposed to contain greater than or equal to 1 cell and thus to be bright. The observed positive  
245 fraction of  $62.0 \pm 1.5\%$  after 4 hours of incubation matched well with the theoretical value of 63%.  
246 It was also noticed that, after 3 hours of incubation, the positive Gelbead fraction was  $36.4 \pm 8.1\%$ ,  
247 which corresponds well with the theoretical fraction of Gelbeads (29%) encapsulating more than  
248 1 cell. Based on the linear response of alamarBlue to the number of cells within the compartment  
249 (36), our results reasonably indicate that effective single cell phenotyping in Gelbeads is  
250 achievable within 4 hrs. However, 5 hr incubation lead to overly bright fluorescence and  $92.9 \pm 2.7\%$   
251 bright Gelbeads, which was likely attributed to excessive incubation and the diffusion of  
252 metabolized fluorescent resorufin across the aqueous-oil interfacial barrier. Our results indicate  
253 that the optimization of incubation time is a race between cross-talking and cell proliferation.  
254 Considering the intrinsic difference in proliferation rate between bacterial species, the observed  
255 incubation time for distinction of positive and negative compartments was comparable to the  
256 results by Lyu et al., who achieved *Escherichia coli* (*E. coli*) phenotyping with alamarBlue in 85  
257 pL droplets with a 2 hr incubation (3). We note that, although the single cell encapsulated Gelbeads  
258 were maximized and theoretically comprised the majority (54%) of the bright Gelbeads in the  
259 current set up, strategies are available to break Poisson distribution for higher single cell  
260 encapsulation rates, such as microvortex-aided hydrodynamic trapping and then releasing single

261 cells to droplets (37). In summary, the cell viability detection strategy demonstrated with Gelbeads  
262 has been proved to apply well to a wide range of cells in bulk assays and droplet microfluidics (3,  
263 34, 36). Thus, the Gelbeads synthesized in this study provide a suitable platform for phenotyping  
264 cell heterogeneity, if they are co-encapsulated with antibiotics or drugs.

## Discussion

265 The developed Gelbeads platform promises a robust analysis tool that has the potential to  
266 link single-cell phenotypic analysis with reliable *in situ* molecular detection together. Besides the  
267 advantages presented, we acknowledge the following limitations. First, the dynamic range in our  
268 study was restricted by the size of the compartments generated by our device. Further reductions  
269 in size would result in larger size variations, and the surfactant might have to be changed or  
270 adjusted if higher uniformity is required. Second, given the use of fluorescence microscopic  
271 imaging of the compartments inside a viewing chamber, the Gelbead imaging approach employed  
272 could probe only a limited viewing area, and the resolution could be affected by the focus. The  
273 fluorescence characterization may be further improved by flow cytometry to interrogate single  
274 Gelbeads.

275 In this work, a disposable centrifugal device was developed for Gelbead generation using  
276 highly biocompatible PEG monomers spontaneously crosslinked with no free-radical, UV-induced  
277 or heat-induced initiation. Our design allows for easy use of droplet microfluidics without  
278 expensive and complicated equipment, which could be useful for applications other than Gelbeads  
279 generation. In addition to the single cell phenotyping potential, the Gelbeads approach has  
280 enhanced thermal stability coupled with high amplification efficiency for dPCR and dLAMP.  
281 Widely available qPCR and LAMP assays can therefore be easily transferred into digital assays  
282 by this Gelbeads approach. The unique structural stability of the hydrogel network allows for easy

283 manipulation of the Gelbeads that may have many possibilities for other upstream and downstream  
284 analyses. The Gelbead platform will be further developed for reagent exchange, fluorescence-  
285 based Gelbead sorting, and downstream sequencing, etc. We envision that the potential of our  
286 Gelbeads platform in generating genetic and gene expression data with phenotyped single cells  
287 will help narrow the genotype-phenotype gap and thus offer exciting new insights in cell  
288 heterogeneity studies.

## Materials and Methods

### 289 **PEG crosslinking and characterizations**

290 PEG hydrogel monomers included 4-arm PEG-acrylate [molecular weight (MW) of 10 000,  
291 Laysan Bio, Arab, AL, USA] and thiol-PEG-thiol (MW of 3400; Laysan Bio), with acrylate and  
292 thiol mixed at a molar ratio of 1:1 for crosslinking. For sol-gel transition time characterization, 7.5  
293 w/v% and 10 w/v% PEG hydrogel were respectively tested in PCR mix, LAMP mix, and culture  
294 media mix. PEG monomers were weighed to make 10× monomer solutions for PEG-acrylate and  
295 PEG-thiol separately. The weighed monomers were then dissolved either in water (Molecular  
296 Biology Grade Water, Corning, Acton, MA, USA) for PCR and LAMP mix, or in TSB (BD™  
297 Bacto™ Tryptic Soy Broth, Becton Dickinson and Company, Franklin Lakes, NJ, USA) for culture  
298 media mix. In addition to 2 µL of each 10× PEG monomer solution, for each 20 µL reaction mix,  
299 PCR mix contained 10 µL ddPCR Supermix for Probes (BioRad, Hercules, CA, USA) and 6 µL  
300 water; LAMP mix contained 10 µL 2×WarmStart LAMP Mastermix (New England Biolabs,  
301 Ipswich, MA, USA) and 6 µL water; culture media mix contained 16 µL TSB. The reaction mix  
302 was briefly vortexed. The sol-gel transition was considered started when lifting the pipette tip  
303 could draw filaments out of the reaction mix, and the transition was considered ended when the  
304 reaction mix formed a gelatinous lump.

### 305 **Development of the disposable droplet generation device**

306 Each droplet generation device consisted of a 1.5 mL DNA LoBind tube (Eppendorf,  
307 Hamburg, Germany) and a blunt tip dispensing needle (LAOMA Amazon, Seattle, WA, USA)  
308 with the tip bent by a tweezer (VWR, Radnor, PA, USA). The tweezer and the needles were  
309 autoclaved (2540EP, Heidolph Brinkmann, Schwabach, Germany) prior to use. The oil phase was  
310 added to the bottom of the microcentrifuge tube, and the aqueous reaction mix was added to the

311 Luer-lock of the needle. The device was then centrifuged (Centrifuge 5430R, Eppendorf) for 5  
312 min. For optimization of droplet generation, fluorinated oil (HFE-7500 3M<sup>®</sup> Novec<sup>®</sup> Engineering  
313 Fluid, 3M, Maplewood, MN, USA) supplied with 5% FluoroSurfactant (RAN Biotechnologies,  
314 Beverly, MA, USA) was added into the oil phase. The 20- $\mu$ L aqueous phase contained  
315 1 $\times$ WarmStart LAMP Mastermix and 50  $\mu$ M calcein (Sigma-Aldrich, St. Louis, MO, USA). Four  
316 parameters including oil phase volume, needle inner diameter, centrifugal acceleration and oil  
317 volume added to the Luer-lock were investigated. Specific variables in details were as follows: 1)  
318 the oil phase volume of 40, 60, 80 and 100  $\mu$ L, respectively, at the bottom of the tube in 34 Ga  
319 needles under 250 g centrifugation; 2) needles of 30, 32 and 34 Ga (corresponding to inner  
320 diameter of around 160, 110 and 80  $\mu$ m) under the condition of 250 g centrifugation and 80  $\mu$ L oil  
321 phase volume; 3) the centrifugal accelerations of 50, 150, 250, 500, 1000 g with 34 Ga needles  
322 and 80  $\mu$ L oil phase; 4) additional oil phase added into the Luer-lock of 0, 10 and 20  $\mu$ L in 34 Ga  
323 needles under 250 g centrifugation with 80  $\mu$ L oil phase.

#### 324 **Gelbead generation and thermal stability characterization**

325 In all the following experiments, the device configuration was fixed with 34 Ga needles,  
326 80  $\mu$ L oil phase, no additional oil at the Luer-lock, and 150 g centrifugation run for 5 min. The  
327 droplet and Gelbead generation using the described device was respectively characterized with  
328 PCR mix, LAMP mix, and culture media mix. In each 20  $\mu$ L reaction, the PCR mix contained 1 $\times$   
329 ddPCR Supermix and 50  $\mu$ M calcein; the LAMP mix contained 1 $\times$ WarmStart LAMP Mastermix,  
330 and 50  $\mu$ M calcein; the culture media mix was TSB with 1 mg/mL BSA (New England Biolabs)  
331 and 50  $\mu$ M calcein. The mix was briefly pipette mixed. The reaction mix for Gelbead generation  
332 contained 7.5 w/v% PEG hydrogel, added as 10 $\times$  PEG monomers. For dispersion of PCR mix as



333 droplets and Gelbeads, Droplet Generation Oil for Probes (BioRad) was used instead of fluorinated  
334 oil with 5% FluoroSurfactant.

335 For thermal stability characterizations, generated droplets or Gelbeads were extracted into  
336 PCR tubes (0.2 mL individual PCR tubes, BioRad) and incubated in a thermal cycler (T100,  
337 BioRad). The thermocycling protocol for PCR included 10 min of initiation at 95 °C, followed by  
338 40 cycles of denaturation at 94 °C for 30 s, annealing at 52 °C for 60 s, and extension at 65 °C for  
339 30 s. For LAMP heating, droplets or Gelbeads were incubated at 65 °C for 1 hour.

#### 340 **Bacterial Cell culture and DNA preparation**

341 *Salmonella* Typhi (*S. Typhi*, CVD 909), obtained from American Type Culture Collection  
342 (ATCC, Manassas, VA, USA), was employed as the model strain. *S. Typhi* was cultivated in TSB  
343 supplied with 1 mg/L of 2,3-dihydroxybenzoate (DHB, Sigma-Aldrich) in an incubator (Innova  
344 42, New Brunswick Scientific, Edison, NJ, USA) shaking at 200 rpm at 35 °C for 14-16 hours.  
345 The concentration of cultivated cells was estimated by OD 600 (NanoDrop 2000c  
346 Spectrophotometer, Thermo Scientific, Barrington, IL, USA). DNA was harvested using  
347 PureLink® Genomic DNA Mini Kits (Fisher Scientific, Waltham, MA, USA) following the  
348 manufacturer's instructions. For single cell encapsulation test, *Salmonella* Typhimurium GFP  
349 (ATCC 14028GFP) was cultivated in nutrient broth (Difco™ 23400, Becton Dickinson and  
350 Company) supplied with 100 mcg/ml Ampicillin (Sigma-Aldrich) in an incubator shaking at 200  
351 rpm at 37 °C for 14-16 hours. The cell concentration was estimated by counting under a  
352 fluorescence microscope (Leica DMI8, Wetzlar, Germany).

#### 353 **Gelbead Digital PCR (gdPCR) assay**

354 The thermocycling protocol of gdPCR assay was the same as described in the thermal  
355 stability characterization. Each 20 µL reaction consisted of 1× ddPCR Supermix, 900 nM forward

356 primer, 900 nM reverse primer, 250 nM probe, and 2  $\mu$ L DNA sample or water. Additional 7.5  
357 w/v% PEG hydrogel was added as 10 $\times$  PEG monomers for gdPCR assays. The primers and probe  
358 were ordered from Integrated DNA Technologies (IDT, Coralville, IA, USA), with sequences  
359 (**Supplementary Table S1**) designed for specific detection of *S. Typhi*, targeting a region in gene  
360 STY0201 for an amplicon size of 131 bp (32). For gdPCR optimization, the same DNA template  
361 concentration (600 times dilution from harvested) was added for gdPCR assays and ddPCR control.  
362 Optimal concentration of additional polymerase (OneTaq<sup>®</sup> DNA polymerase, New England  
363 Biolabs) was investigated by supplying various concentrations to the described reaction mix  
364 incrementally at 0.025, 0.5, 0.1 and 0.2 U/reaction. For quantification assays, harvested DNA  
365 sample were serial diluted 100, 300, 600, 1500, and 24000 times for ddPCR and gdPCR. The  
366 reactions were prepared on iceblock (Carolina<sup>®</sup> Chill Block, Burlington, NC, USA) and  
367 centrifugation temperature was set at 4  $^{\circ}$ C. Droplets or Gelbeads were generated in BioRad droplet  
368 generation oil, and were then extracted into PCR tubes for thermocycling. No-template controls  
369 were examined for each tested condition.

#### 370 **Gelbead Digital LAMP (gdLAMP) assay**

371 The reagents for LAMP were acquired from New England BioLabs if not indicated  
372 otherwise. Each 20  $\mu$ L of modified LAMP mix for digital single bacteria LAMP contained 1 $\times$   
373 isothermal buffer, 6 mM total MgSO<sub>4</sub>, 1.4 mM dNTP, 640 U/mL Bst 2.0 WarmStart polymerase,  
374 1.6  $\mu$ M FIB and BIP, 0.2  $\mu$ M F3 and B3, 0.8  $\mu$ M LF and LB, 1.5 mg/mL BSA, 1 $\times$  LAMP dye (38).  
375 For gdLAMP assays, 7.5 w/v% PEG hydrogel was added as 10 $\times$  PEG monomers. The primers,  
376 ordered from IDT with the sequences shown in **Supplementary Table S1**, were targeting a 196  
377 bp region within the *S. Typhi* specific gene STY1607 (39). For gdLAMP and ddLAMP assays,  
378 harvested DNA was serial diluted 5, 20, 50, 100, and 200 times. The reactions were prepared on

379 iceblock and centrifuged into 5% FluoroSurfactant supplied fluorinated oil at 4 °C. Droplets or  
380 Gelbeads were then extracted into PCR tubes for 30 min heating at 65 °C followed by 5 min  
381 polymerase deactivation at 80 °C. No-template controls were examined under the same protocol.

### 382 **Single cell phenotyping**

383 For single cell encapsulation efficiency test, the cultivated *Salmonella* Typhimurium GFP  
384 was diluted 600 times for Gelbeads generation. The dilution factor was estimated from prior  
385 knowledge of cultured cell concentration and Gelbead volume. The number of cells encapsulated  
386 in each Gelbead was analyzed by fluorescence microscope imaging with a 20× objective. 79  
387 Gelbeads were analyzed from 15 fluorescent images. For phenotyping experiments, 1mL of  
388 overnight cultured *S. Typhi* was freshly cultivated for 3 hours in 5mL TSB supplied with 1 mg/L  
389 of DHB in an incubator shaking at 200 rpm at 35 °C. The cell concentration was verified to be  
390 around 0.135 by OD 600. AlamarBlue (Invitrogen, Carlsbad, CA, USA) was employed as the cell  
391 viability indicator. To address the fluctuation of excitation intensity and emission detection within  
392 a microscopic view, calcein was used as a reference dye. Each 20 µL reaction consisted of 1×  
393 AlamarBlue, 50 µM calcein, 1 mg/mL BSA, diluted *S. Typhi* cells, and the rest of the volume filled  
394 with DHB supplied TSB. 7.5 w/v% PEG hydrogel was added as 10× PEG monomers dissolved in  
395 DHB supplied TSB. After generation, the Gelbeads were incubated at 37 °C for 0-5 hrs. Gelbeads  
396 were extracted for imaging after 0, 1, 2, 3, 4 hrs of incubation.

### 397 **Droplets and Gelbeads imaging and analysis**

398 The droplets or Gelbeads to be analyzed were pipetted into a viewing chamber made by  
399 adhering SecureSeal™ Hybridization Chamber (9 mm DIA × 1.0 mm Depth, Grace Bio-Labs,  
400 Bend, OR, USA) to a glass slide (VistaVision® Microscope slides, VWR). The chambers were  
401 imaged under the fluorescence microscope using a 1.25× objective for droplets/Gelbeads

402 generation, characterizations, and gdLAMP. For each sample in gdPCR and single cell  
403 phenotyping, five images of different area in the viewing chamber were taken using a 5× objective.  
404 Fluorescein isothiocyanate (FITC) filter was used, except for phenotyping experiments where  
405 Texas Red (TXR) filter was used in addition. In phenotyping experiments, the image data collected  
406 through TXR channel was normalized using the image data collected through FITC channel. For  
407 analysis of bright Gelbeads fraction, the data of each pixel was the intensity ratio of TXR channel  
408 to FITC channel. All images were analyzed using customized MATLAB scripts (**Supplementary**  
409 **Files**). For droplets and Gelbeads generation as well as thermal stability characterizations, the  
410 images were analyzed for individual compartment diameters. The diameters were further analyzed  
411 to calculate average compartment diameter and coefficient of variation (CV). For gdPCR,  
412 gdLAMP, and phenotyping assays, in addition to size analysis, the images were also analyzed for  
413 number of positive and negative compartments by setting a bright-dark threshold. Using the ratio  
414 of negative compartments to total compartments, the input DNA or cell concentrations were  
415 estimated by Poisson distribution (40). For images from phenotyping assays, since the distinction  
416 of dark and bright Gelbeads was hard to inspect visually, Gaussian fitting was used to advice the  
417 threshold (**Figure S5**).

## Reference

- 418 1. C. M. O'Keefe *et al.*, Facile profiling of molecular heterogeneity by microfluidic digital melt. *Sci*  
419 *Adv* **4**, (2018).
- 420 2. L. F. Cheow *et al.*, Single-cell multimodal profiling reveals cellular epigenetic heterogeneity. *Nat*  
421 *Methods* **13**, 833-836 (2016).
- 422 3. F. J. Lyu *et al.*, Phenotyping antibiotic resistance with single-cell resolution for the detection of  
423 heteroresistance. *Sensor Actuat B-Chem* **270**, 396-404 (2018).
- 424 4. I. El Meouche, M. J. Dunlop, Heterogeneity in efflux pump expression predisposes antibiotic-  
425 resistant cells to mutation. *Science* **362**, 686+ (2018).
- 426 5. D. Shibata, Cancer. Heterogeneity and tumor history. *Science* **336**, 304-305 (2012).
- 427 6. D. I. Andersson, H. Nicoloff, K. Hjort, Mechanisms and clinical relevance of bacterial  
428 heteroresistance. *Nat Rev Microbiol*, (2019).
- 429 7. U. Ben-David *et al.*, Genetic and transcriptional evolution alters cancer cell line drug response.  
430 *Nature* **560**, 325-330 (2018).
- 431 8. A. Harms, E. Maisonneuve, K. Gerdes, Mechanisms of bacterial persistence during stress and  
432 antibiotic exposure. *Science* **354**, (2016).
- 433 9. H. Nicoloff, K. Hjort, B. R. Levin, D. I. Andersson, The high prevalence of antibiotic  
434 heteroresistance in pathogenic bacteria is mainly caused by gene amplification. *Nat Microbiol* **4**,  
435 504-514 (2019).
- 436 10. V. Takhaveev, M. Heinemann, Metabolic heterogeneity in clonal microbial populations. *Curr Opin*  
437 *Microbiol* **45**, 30-38 (2018).
- 438 11. E. A. Ottesen, J. W. Hong, S. R. Quake, J. R. Leadbetter, Microfluidic digital PCR enables  
439 multigene analysis of individual environmental bacteria. *Science* **314**, 1464-1467 (2006).
- 440 12. A. Marusyk, V. Almendro, K. Polyak, Intra-tumour heterogeneity: a looking glass for cancer? *Nat*  
441 *Rev Cancer* **12**, 323-334 (2012).

- 442 13. Y. S. Zhang, A. Khademhosseini, Advances in engineering hydrogels. *Science* **356**, (2017).
- 443 14. Z. Zhu *et al.*, Highly sensitive and quantitative detection of rare pathogens through agarose droplet  
444 microfluidic emulsion PCR at the single-cell level. *Lab on a Chip* **12**, 3907-3913 (2012).
- 445 15. W. H. Tan, S. Takeuchi, Monodisperse alginate hydrogel microbeads for cell encapsulation.  
446 *Advanced Materials* **19**, 2696-+ (2007).
- 447 16. P. Zimny, D. Juncker, W. Reisner, Hydrogel droplet single-cell processing: DNA purification,  
448 handling, release, and on-chip linearization. *Biomicrofluidics* **12**, (2018).
- 449 17. C. J. Young, L. A. Poole-Warren, P. J. Martens, Combining submerged electrospray and UV  
450 photopolymerization for production of synthetic hydrogel microspheres for cell encapsulation.  
451 *Biotechnol Bioeng* **109**, 1561-1570 (2012).
- 452 18. H. Ikehata, T. Ono, The Mechanisms of UV Mutagenesis. *J Radiat Res* **52**, 115-125 (2011).
- 453 19. R. M. Wadowsky, S. Laus, T. Libert, S. J. States, G. D. Ehrlich, Inhibition of Pcr-Based Assay for  
454 Bordetella-Pertussis by Using Calcium Alginate Fiber and Aluminum Shaft Components of a  
455 Nasopharyngeal Swab. *Journal of Clinical Microbiology* **32**, 1054-1057 (1994).
- 456 20. L. Xu, I. L. Brito, E. J. Alm, P. C. Blainey, Virtual microfluidics for digital quantification and  
457 single-cell sequencing. *Nat Methods* **13**, 759-762 (2016).
- 458 21. X. Huang *et al.*, Smartphone-Based in-Gel Loop-Mediated Isothermal Amplification (gLAMP)  
459 System Enables Rapid Coliphage MS2 Quantification in Environmental Waters. *Environ Sci*  
460 *Technol* **52**, 6399-6407 (2018).
- 461 22. F. Schuler *et al.*, Centrifugal step emulsification applied for absolute quantification of nucleic acids  
462 by digital droplet RPA. *Lab on a Chip* **15**, 2759-2766 (2015).
- 463 23. Y. C. Tan, V. Cristini, A. P. Lee, Monodispersed microfluidic droplet generation by shear focusing  
464 microfluidic device. *Sensor Actuat B-Chem* **114**, 350-356 (2006).
- 465 24. S. Haeberle *et al.*, Alginate bead fabrication and encapsulation of living cells under centrifugally  
466 induced artificial gravity conditions. *J Microencapsul* **25**, 267-274 (2008).

- 467 25. J. E. Kreutz *et al.*, Theoretical design and analysis of multivolume digital assays with wide dynamic  
468 range validated experimentally with microfluidic digital PCR. *Anal Chem* **83**, 8158-8168 (2011).
- 469 26. G. L. Francis, Albumin and mammalian cell culture: implications for biotechnology applications.  
470 *Cytotechnology* **62**, 1-16 (2010).
- 471 27. R. D. Mitra, G. M. Church, In situ localized amplification and contact replication of many  
472 individual DNA molecules. *Nucleic Acids Res* **27**, (1999).
- 473 28. S. J. Spencer *et al.*, Massively parallel sequencing of single cells by epicPCR links functional genes  
474 with phylogenetic markers. *Isme J* **10**, 427-436 (2016).
- 475 29. R. Zilionis *et al.*, Single-cell barcoding and sequencing using droplet microfluidics. *Nature*  
476 *Protocols* **12**, (2017).
- 477 30. L. M. Weber, C. G. Lopez, K. S. Anseth, Effects of PEG hydrogel crosslinking density on protein  
478 diffusion and encapsulated islet survival and function. *J Biomed Mater Res A* **90a**, 720-729 (2009).
- 479 31. Y. B. Wu, S. Joseph, N. R. Aluru, Effect of Cross-Linking on the Diffusion of Water, Ions, and  
480 Small Molecules in Hydrogels. *J Phys Chem B* **113**, 3512-3520 (2009).
- 481 32. V. T. N. Tran *et al.*, The sensitivity of real-time PCR amplification targeting invasive Salmonella  
482 serovars in biological specimens. *Bmc Infectious Diseases* **10**, (2010).
- 483 33. T. Notomi *et al.*, Loop-mediated isothermal amplification of DNA. *Nucleic Acids Res* **28**, E63  
484 (2000).
- 485 34. M. L. Xu, D. J. McCanna, J. G. Sivak, Use of the viability reagent PrestoBlue in comparison with  
486 alamarBlue and MTT to assess the viability of human corneal epithelial cells. *J Pharmacol Tox*  
487 *Met* **71**, 1-7 (2015).
- 488 35. B. H. Neufeld, J. B. Tapia, A. Lutzke, M. M. Reynolds, Small Molecule Interferences in Resazurin  
489 and MTT-Based Metabolic Assays in the Absence of Cells. *Anal Chem* **90**, 6867-6876 (2018).
- 490 36. J. Shemesh *et al.*, Stationary nanoliter droplet array with a substrate of choice for single  
491 adherent/nonadherent cell incubation and analysis. *Proc Natl Acad Sci U S A* **111**, 11293-11298  
492 (2014).

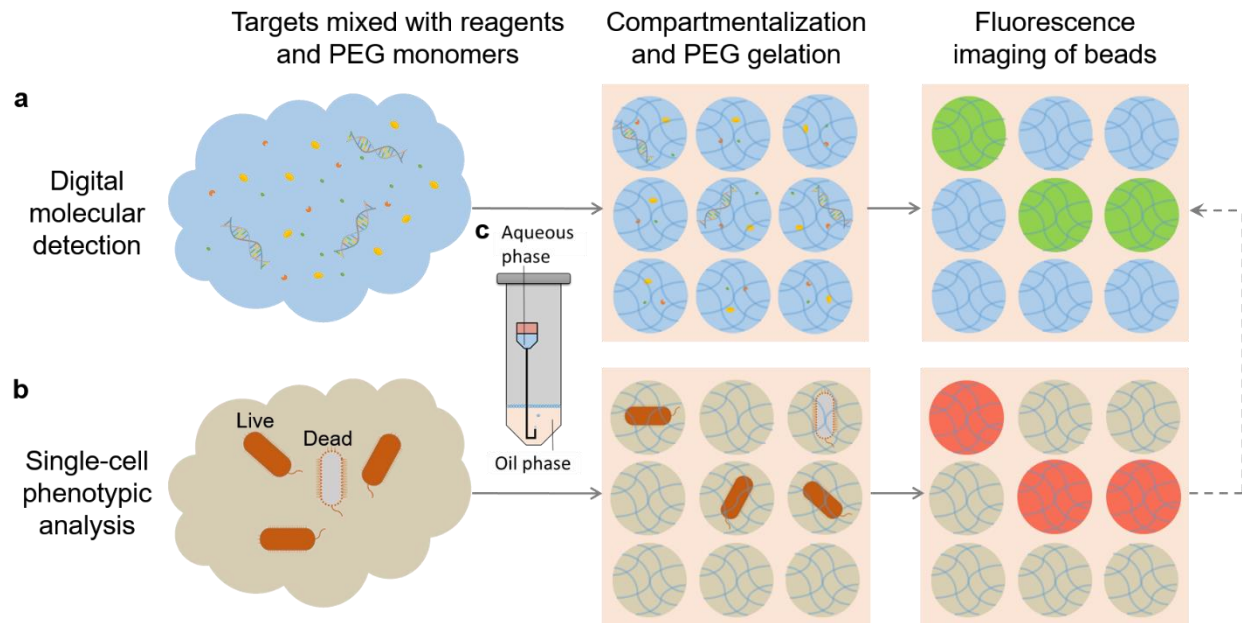
- 493 37. E. Um, S. G. Lee, J. K. Park, Random breakup of microdroplets for single-cell encapsulation. *Appl*  
494 *Phys Lett* **97**, (2010).
- 495 38. X. Lin, X. Huang, K. Urmann, X. Xie, M. R. Hoffmann, Digital Loop-Mediated Isothermal  
496 Amplification on a Commercial Membrane. *ACS Sens* **4**, 242-249 (2019).
- 497 39. F. X. Fan, M. Y. Yan, P. C. Du, C. Chen, B. Kan, Rapid and Sensitive Salmonella Typhi Detection  
498 in Blood and Fecal Samples Using Reverse Transcription Loop-Mediated Isothermal Amplification.  
499 *Foodborne Pathogens and Disease* **12**, 778-786 (2015).
- 500 40. L. B. Pinheiro *et al.*, Evaluation of a Droplet Digital Polymerase Chain Reaction Format for DNA  
501 Copy Number Quantification. *Analytical Chemistry* **84**, 1003-1011 (2012).
- 502



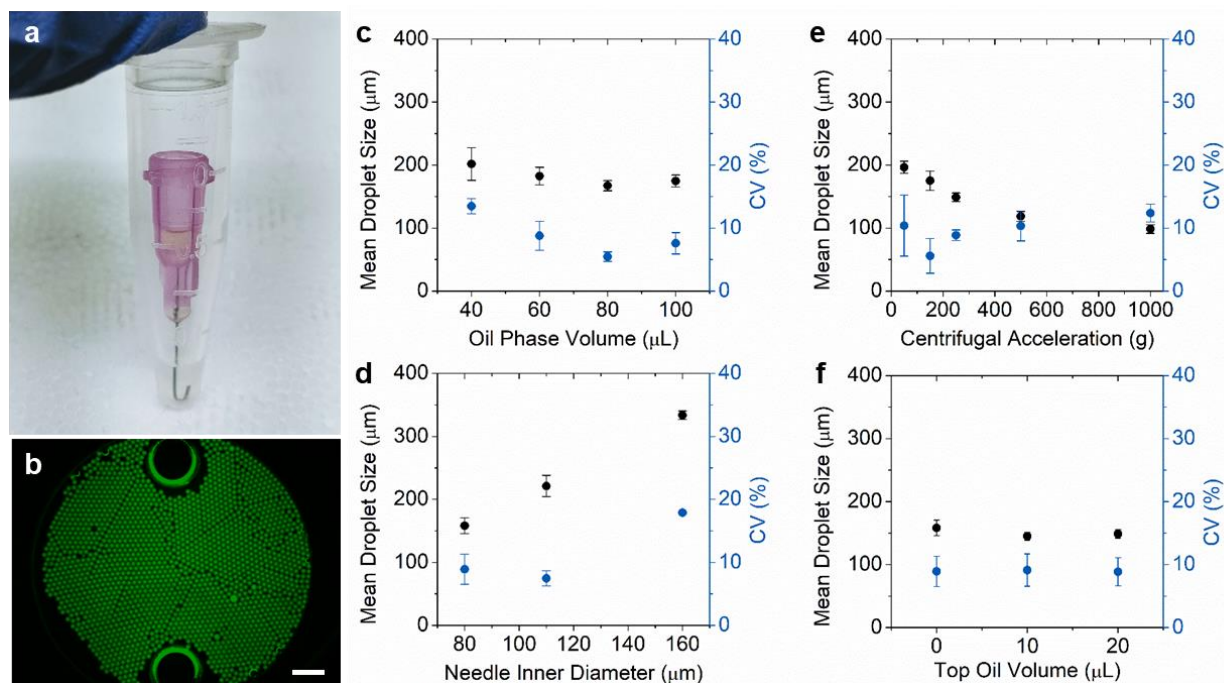
503 **Acknowledgment:**

504 **General:** We thank Dr. Katharina Urmann for helpful discussions. **Funding:** The authors  
505 acknowledge the financial support provided by the Bill and Melinda Gates Foundation (grant nos.  
506 OPP1111252 and OPP1192379). **Author contributions:** The manuscript was written through  
507 contributions of all authors. M.R.H, X.H., and Y.Z. conceived the concept for this study. J.L.,  
508 X.H., X.L. and Y.Z. designed the study, Y.Z. performed experiments, and J.L. and Y.Z. wrote the  
509 paper. All authors approved of the manuscript. **Competing interests:** The authors declare no  
510 competing financial interests. **Data and materials availability:** The manuscript and the  
511 supplementary materials contain all data needed to evaluate the conclusions in the paper.  
512 Correspondence and requests for materials should be addressed to M.R.H.

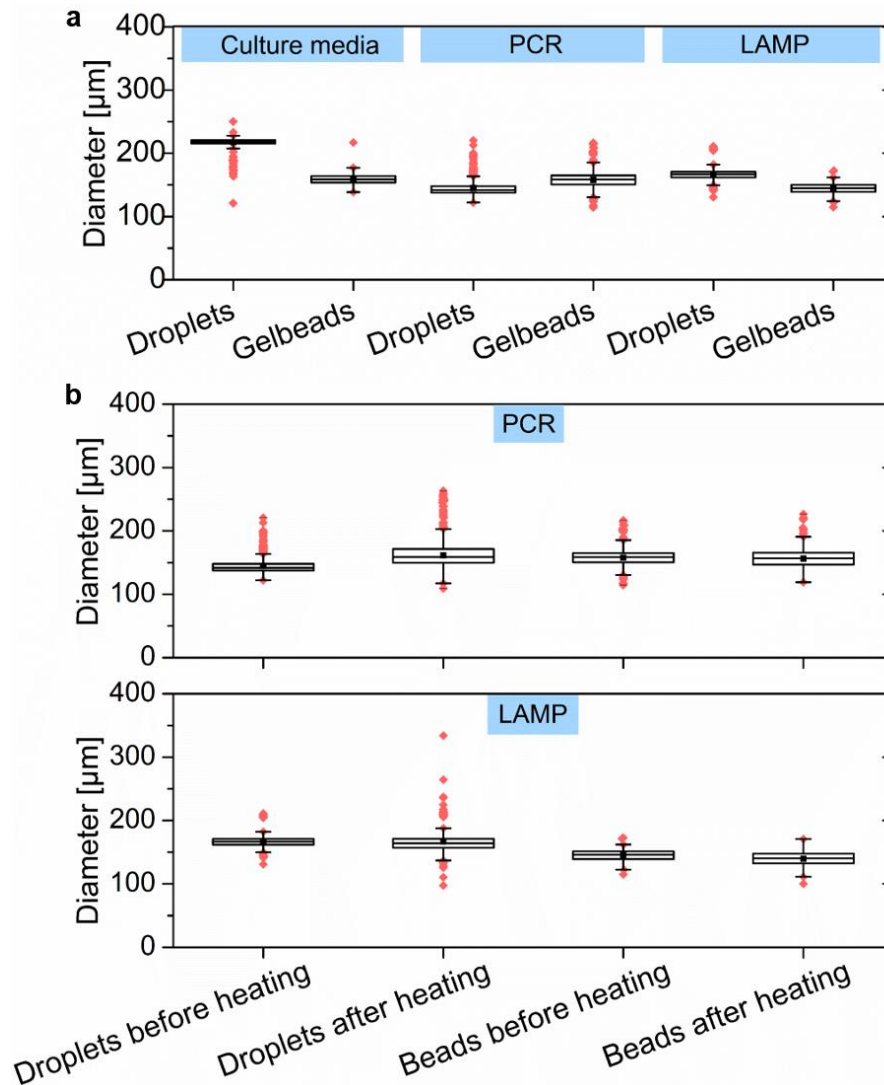
## Display Items



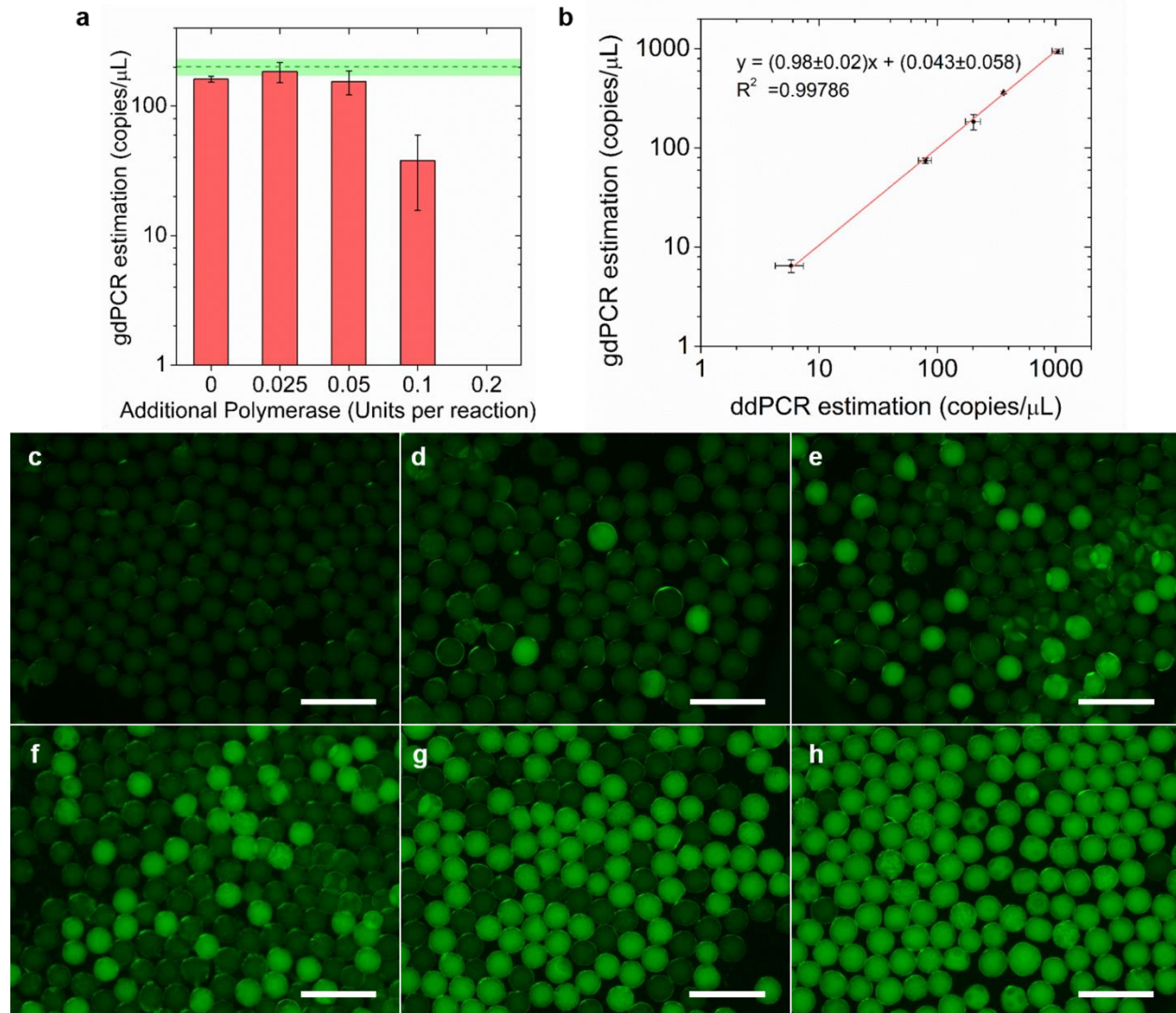
513 **Figure 1. Schematic of this study.** A hydrogel bead (Gelbeads)-based cell analysis platform was  
514 developed for (a) digital molecular detection including PCR and LAMP and (b) single-cell  
515 phenotypic analysis. The compartmentalization was realized by (c) a disposable centrifugal droplet  
516 generation device. The dashed-line arrow indicates that the crosslinked hydrogel network grants  
517 the potential of linking cell phenotype with *in situ* DNA/RNA characterization at single-cell  
518 resolution.



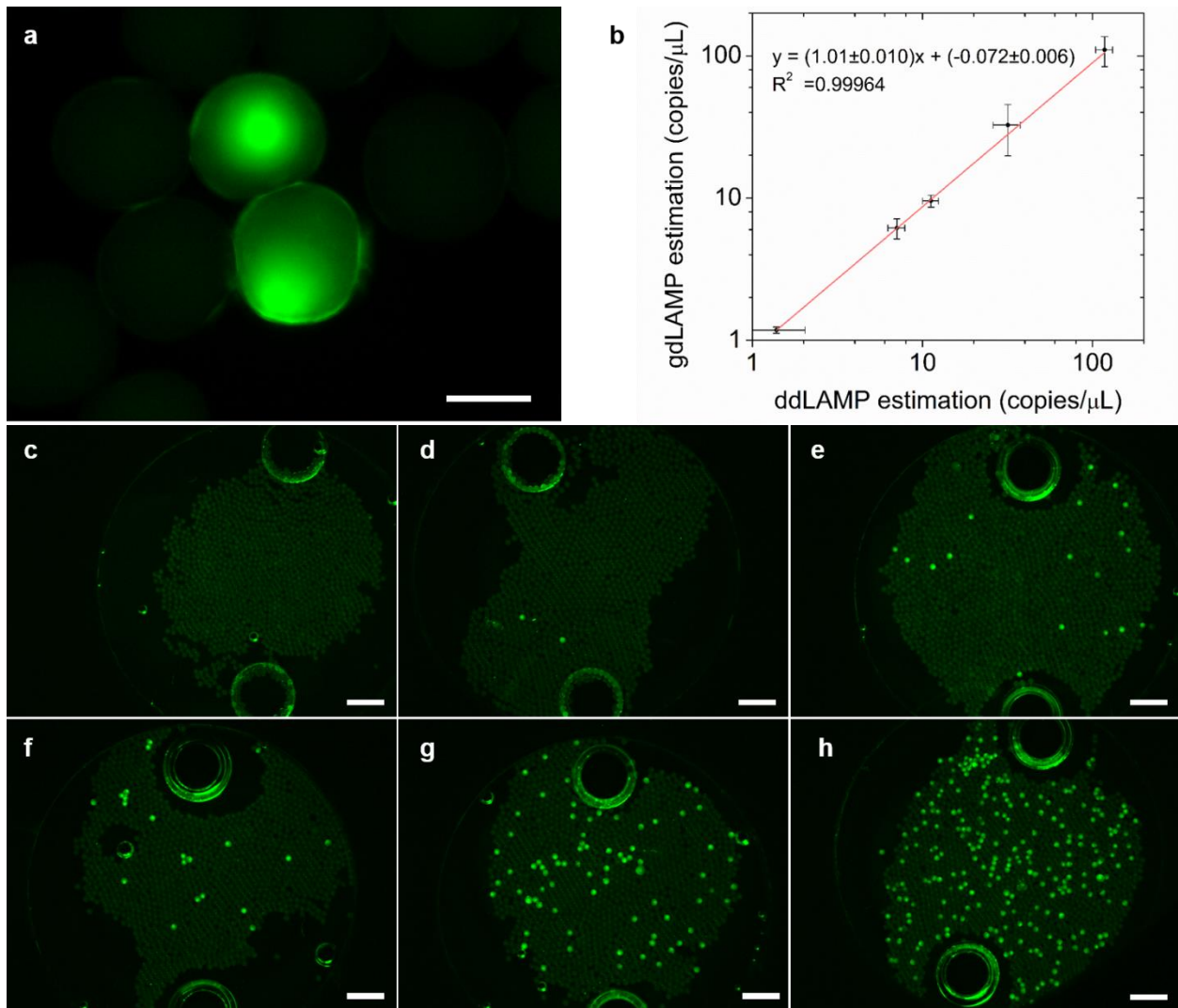
519 **Figure 2. Development and evaluation of disposable microfluidics for centrifugal droplet**  
520 **generation.** (a) The device setup consisting of a 1.5-mL microcentrifuge tube holding the oil phase  
521 and a needle with bent tip holding the aqueous reaction mixture in the Luer-lock. (b) A  
522 representative fluorescence microscope image of generated droplets extracted into a viewing  
523 chamber. The two large bright circles are ports on the viewing chamber for liquid loading Scale  
524 bar, 1 mm. (c-f) Mean droplet size (black circles) and CV (blue circles) of droplets produced under  
525 varying parameters including (c) oil phase volume, (d) needle inner diameter, (e) centrifugal  
526 acceleration and (f) oil volume added to the Luer-lock. Error bars represent standard deviation  
527 from independent triplicates.



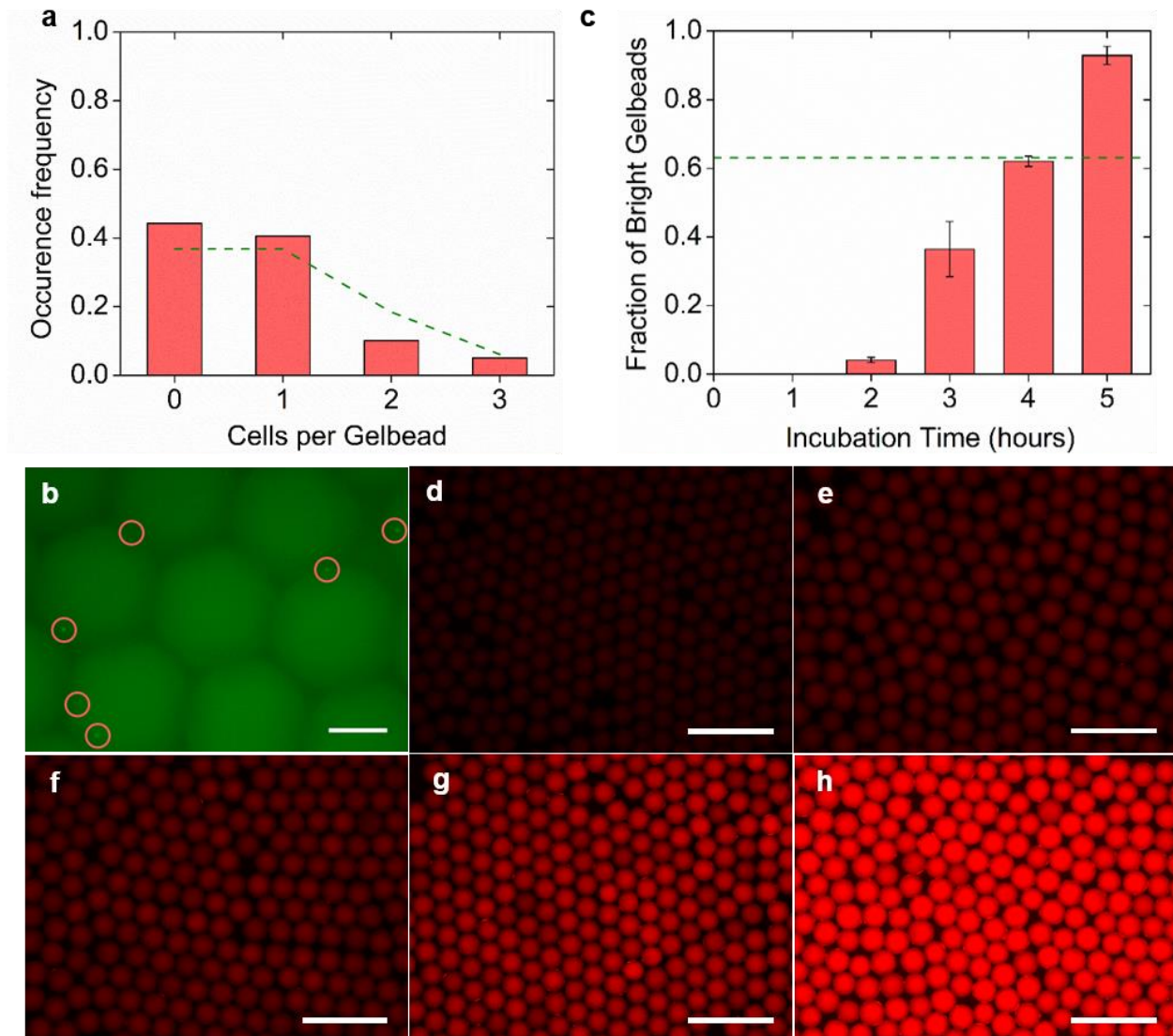
528 **Figure 3. Size characterization of droplets and Gelbeads.** The size distribution of droplets and  
529 Gelbeads (a) generated in reaction matrices including PCR mix, LAMP mix, and culture media  
530 mix, and (b) before and after heating program designated for PCR and LAMP. The line inside  
531 each box represents the mean diameter; the lower and upper edges of each box respectively  
532 represent 25% and 75% percentiles; the vertical bars below and above each box respectively  
533 indicate 90<sup>th</sup> and 10<sup>th</sup> percentiles. The lower and upper red dots stand for outliers.



534 **Figure 4. Optimization and performance of gdPCR.** (a) The concentration estimations of  
535 gdPCR assays for a fixed input *S. Typhi* DNA concentration (200 copies/μL) with varying  
536 concentrations of additional polymerase. The green dashed line and the green area represent mean  
537 concentration estimation with standard deviation of ddPCR assays from independent triplicates.  
538 (b) With the optimized additional polymerase concentration (0.025 Units per reaction), the  
539 correlation between gdPCR and ddPCR estimation for serial diluted target templates. Error bars  
540 represent standard deviations from independent triplicates. (c-h) Example gdPCR fluorescent  
541 images for no DNA input, and with 24000, 1500, 600, 300, 100 times dilution of harvested *S.*  
542 *Typhi* DNA. Scale bars, 500 μm.



543 **Figure 5. Performance of gdLAMP.** (a) Connection of two positive Gelbeads after the gdLAMP  
544 assay. Scale bar, 100  $\mu$ m. (b) The correlation between concentration estimations of gdLAMP and  
545 ddLAMP assays for serial diluted target templates. Error bars represent standard deviation from  
546 independent triplicates. (c-h) Example gdLAMP fluorescent images for no DNA input, and with  
547 200, 100, 50, 20, 5 times dilution of harvested *S. Typhi* DNA. The two large bright circles on each  
548 image are ports on the viewing chamber for liquid loading. Scale bars, 500  $\mu$ m.



549 **Figure 6. Single cell encapsulation validation and Single cell phenotyping performance in**  
550 **Gelbeads.** (a) Number of cells encapsulated in each Gelbead counted and represented by  
551 occurrence frequency. The dashed line represent theoretical values based on Poisson distribution.  
552 (b) Example fluorescence image of encapsulated *S. Typhimurium* GFP cells (circled) for counting.  
553 Scale bar, 100  $\mu\text{m}$ . (c) The observed fraction of bright Gelbeads with varying incubation time,  
554 with the dashed line representing 63% as Poisson distribution predicted based on the input cell  
555 concentration. Error bars represent standard deviation from independent triplicates. (d-h) Example  
556 images of Gelbeads containing *S. typhi* at the same input concentration incubated for 0, 2, 3, 4, 5  
557 hrs. Scale bars, 500  $\mu\text{m}$ .